Anal Bioanal Chem
DOI 10.1007/s00216-017-0420-9

RESEARCH PAPER

Fluorescence turn-on detection of alkaline phosphatase activity based on controlled release of PEI-capped Cu nanoclusters from MnO_2 nanosheets

Yunyi Zhang[1,2,3] · Yongxin Li[2] · Cuiyun Zhang[1,2,3] · Qingfeng Zhang[2,3] · Xinan Huang[2] · Meiding Yang[2,3] · Sohail Anjum Shahzad[2,4] · Kenneth Kam-Wing Lo[5] · Cong Yu[2,3] · Shichun Jiang[1]

Received: 25 January 2017 / Revised: 16 April 2017 / Accepted: 16 May 2017

Abstract A fluorescence turn-on assay for alkaline phosphatase (ALP) activity is developed through the controlled release of polyethyleneimine-capped copper nanoclusters (PEI-capped CuNCs) from the MnO_2 nanosheets. In an aqueous solution, the positively charged PEI-capped CuNCs could be adsorbed onto the surface of the negatively charged MnO_2 nanosheets. Such adsorption through favorable electrostatic interactions could efficiently quench the nanocluster fluorescence emission via resonance energy transfer from the PEI-capped CuNCs to the MnO_2 nanosheets. 2-Phospho-L-ascorbic acid (AAP) could be hydrolyzed to L-ascorbic acid (AA) in the presence of ALP. AA could reduce MnO_2 into Mn^{2+} and trigger the disintegration of the MnO_2 nanosheets. As a result, the CuNCs were released and the quenched fluorescence was recovered efficiently. The detection strategy is simple, inexpensive, sensitive, selective, with low toxicity, and has better biocompatibility. The newly fabricated biosensor for ALP activity will potentially make it a robust candidate for numerous biological and biomedical applications.

Keywords Enzyme activity · MnO_2 nanosheets · Alkaline phosphatase · Cu nanoclusters · Fluorescence assay

Introduction

Alkaline phosphatase (ALP) is an essential enzyme in phosphate metabolism. It is a type of widely used hydrolase enzyme. The main role of ALP is to get rid of the phosphate functional groups in a variety of biomolecules such as nucleic acids and proteins. ALP is present in a variety of mammalian tissues and plays significant roles in various biological processes in living organisms [1, 2]. ALP has been identified as an important biomarker in the diagnosis of various diseases like diabetes [3], bone disease [4], prostate cancer [5], and liver dysfunction [6]. Consequently, it is essential to exploit simple, sensitive, and selective approaches to detect ALP activity.

In recent years, many sensing systems with high sensitivity and selectivity have been established to detect ALP activity, such as the colorimetry [7, 8], electrochemistry [9, 10], chemiluminescence [11], surface-enhanced Raman scattering [12], and fluorescence [13, 14]-based techniques. Among them, fluorescence methods have several advantages and attractive potentials due to their simplicity, high sensitivity, and real-time detection capability with fast response time. So far, along with traditional organic fluorophores [15, 16], some novel fluorescent nanomaterials including metal nanoclusters and

Electronic supplementary material The online version of this article (doi:10.1007/s00216-017-0420-9) contains supplementary material, which is available to authorized users.

✉ Kenneth Kam-Wing Lo
bhkenlo@cityu.edu.hk

✉ Cong Yu
congyu@ciac.ac.cn

✉ Shichun Jiang
scjiang@tju.edu.cn

[1] School of Materials Science and Engineering, Tianjin University, Tianjin 300072, China

[2] State Key Laboratory of Electroanalytical Chemistry, Changchun Institute of Applied Chemistry, Chinese Academy of Sciences, Changchun, Jilin 130022, China

[3] University of Chinese Academy of Sciences, Beijing 100049, China

[4] Department of Chemistry, COMSATS Institute of Information Technology, Abbottabad 22060, Pakistan

[5] Department of Biology and Chemistry, City University of Hong Kong, Tat Chee Avenue, Kowloon, Hong Kong, China

Published online: 14 June 2017

semiconductor quantum dots [17–19] have been applied to detect ALP activity.

Metal nanoclusters (MNCs) are made up of several metal atoms and developed rapidly in recent years [20–22]. They show outstanding chemical, physical, electrical, and optical properties [23–25]. Acting as promising fluorescent nanomaterials, MNCs show appealing performance such as large Stocks shift, high photostability, low toxicity, and good biocompatibility [26–28]. Compared to noble metals, Cu is quite abundant, much cheaper, and widely used in industry. CuNCs have aroused much interest in recent years for their unique properties and various applications in catalysis, biological imaging, and chemical sensing [29, 30]. However, preparation of uniform and stable CuNCs continues to be a challenge owing to its sensitivity towards oxygen in the air [31, 32].

MnO_2 nanosheets have drawn wide attention recently and found a number of biomedical and energy-related applications, e.g., lithium battery construction, drug delivery, biological sensing, and cell imaging [33–35]. MnO_2 nanosheets have excellent biocompatibility and can be easily modified [36–39]. They show a broad absorption spectrum and intense light absorption which can be used for efficient quenching of the fluorescence emission of nanomaterials [40]. Such unique feature has been utilized for fluorescence sensing and imaging-related applications [41, 42].

Herein, a turn-on fluorescence assay for monitoring ALP activity based on the polyethyleneimine (PEI)-capped CuNCs and the MnO_2 nanosheets is established for the first time. The key points of the sensing strategy are illustrated in Scheme 1. The newly prepared MnO_2 nanosheets are negatively charged which could adsorb the positively charged PEI-capped CuNCs through electrostatic attractive interactions. The broad and intense optical absorption spectrum of the MnO_2 nanosheets overlaps with the emission spectrum of the PEI-capped CuNCs. As expected, the fluorescence of the PEI-capped CuNCs is efficiently quenched by the MnO_2 nanosheets via energy transfer. ALP catalyzes the hydrolysis of 2-phospho-L-ascorbic acid (AAP) to produce L-ascorbic acid (AA). The in situ generated AA could reduce MnO_2 into Mn^{2+} and trigger the disintegration of the MnO_2 nanosheets. As a result, the PEI-capped CuNCs are released from the surface of the nanosheets and the quenched fluorescence is restored. The results corroborate that the restoration in fluorescence intensity of the PEI-capped CuNCs is associated with the ALP concentration.

Experimental section

Materials

Polyethyleneimine branched (PEI, Mw = 10,000, 99%) was purchased from Alfa Aesar (Tianjin, China). ALP was purchased from Takara Biotechnology Co., Ltd. (Dalian, China). 2-Phospho-L-ascorbic acid trisodium salt, acetylcholinesterase (from *Electrophorus electricus*), esterase, lipase, and trypsin were purchased from Sigma (St. Louis, MO, USA). Lysozyme was purchased from Dingguo Biotechnology Co., Ltd. (Beijing, China). L-Ascorbic acid was purchased from Sangon Biotech Co. Ltd. (Shanghai, China). All stock and buffer solutions were prepared using water purified with a Milli-Q A10 filtration system (Millipore, Billerica, MA, USA).

Instrumentation

Emission spectra were acquired using a Fluoromax-4 spectrofluorometer (Horiba Jobin Yvon Inc., USA) with an excitation wavelength of 360 nm. UV–Vis absorption spectra were recorded using a Cary 50 Bio Spectrophotometer (Varian Inc., CA, USA) equipped with a xenon flash lamp. Quartz cuvettes with 10 mm path length and 2 mm window width were used for emission and UV–Vis measurements. Zeta potential measurements were performed with a Zetasizer NanoZS (Malvern Instruments, USA). Atomic force microscopy (AFM) characterization was performed on a Multimode-V (Veeco

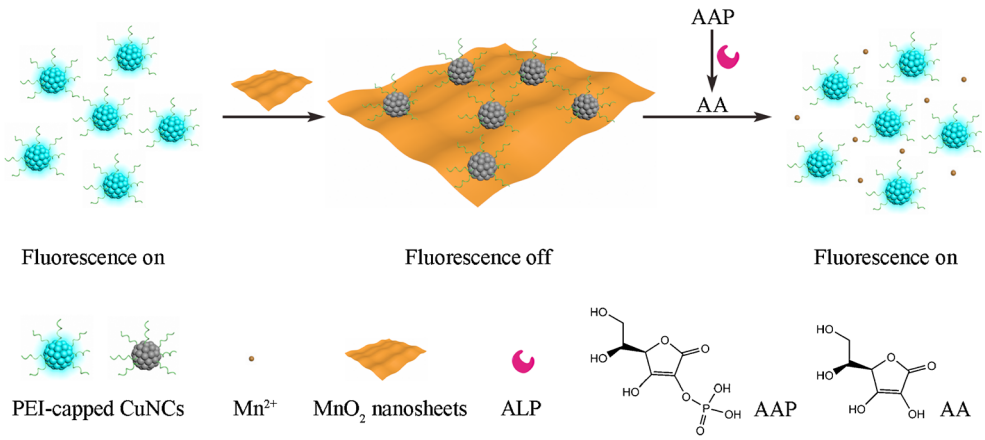

Scheme 1 Schematic illustration of the strategy for the detection of ALP activity

Instruments, USA) using a tapping mode. Transmission electron microscopy (TEM) images were acquired on a JEM-2100F high resolution transmission electron microscope (Philips, The Netherlands) operated at 200 kV. Unless specified, all concentrations of the PEI-capped CuNCs, AAP, MnO_2 nanosheets, and buffer were those in the final assay solutions (total sample volume, 400 μL), and all spectra were measured at 37 °C in 5 mM phosphate buffer at pH 8.2.

Preparation of the PEI-capped CuNCs

The PEI-capped CuNCs were prepared according to the previous report with slight modifications [27]. Firstly, 10 μL of 100 mM $CuSO_4$, 130 μL of 7.7 mM PEI, and 5 mL of water were mixed thoroughly under stirring for 10 min. Then, the pH was adjusted to 5.0 using HAc, and 4 mM of AA was added. The mixture was stirred overnight at room temperature. After that, several milligrams of $NaBH_4$ were added. Finally, the sample mixture was dialyzed for about 12 h to remove the unreacted precursors and small molecular weight by-products.

Preparation of the MnO_2 nanosheets

The MnO_2 nanosheet preparation procedures were adapted from the reported literature method [34]. In a typical experiment, 20 mL of an aqueous solution of 3 wt% H_2O_2 and 0.6 M tetramethylammonium hydroxide was first prepared. Then, 10 mL of 0.3 M $MnCl_2$ solution was added rapidly. The resulting suspension was stirred vigorously overnight in the open air at room temperature. The bulk manganese dioxide was obtained though centrifugation, washed with water and methanol, and dried in an oven. The MnO_2 nanosheets were prepared via ultrasonication of the aqueous solution of the bulk manganese dioxide.

Fluorescence quenching of the PEI-capped copper clusters by MnO_2 nanosheets

Different amounts of the MnO_2 nanosheets (0, 13.75, 27.5, 41.25, 55, 68.75, 82.5, 96.25, 110, 123.75, 137.5, 151.25, and 165 μg/mL, respectively) were added to the solution of the PEI-capped copper nanoclusters (10 μL) in 5 mM phosphate buffer (pH 8.2). The solutions were mixed thoroughly and the emission spectra were taken.

2-Phospho-L-ascorbic acid concentration optimization

Sample mixtures of the total volume of 390 μL including the MnO_2 nanosheets (55 μg/mL), phosphate buffer (5 mM, pH 8.2) and AAP of different concentrations (0.2, 0.4, 0.6, 0.8, and 1 mM, respectively) in the presence and absence of ALP (10 mU/mL) were incubated at 37 °C for 60 min. Then, ten microliters of the PEI-capped copper nanoclusters was added. The samples were mixed and the fluorescence signals were collected.

Sensing of alkaline phosphatase activity

Sample mixtures of the total volume of 390 μL including the MnO_2 nanosheets (55 μg/mL), AAP (0.8 mM), phosphate buffer (5 mM, pH 8.2), and ALP of different concentrations (0, 0.5, 1.0, 5.0, 10.0, 25.0, 50.0, 100.0, and 200.0 mU/mL, respectively) were incubated at 37 °C for a certain period of time (0~80 min). Ten microliters of the PEI-capped copper nanoclusters was added. The resulting solutions were mixed and the fluorescence signals were measured.

Selectivity of the alkaline phosphatase assay

The sample mixtures containing the MnO_2 nanosheets (55 μg/mL), AAP (0.8 mM), phosphate buffer (5 mM, pH 8.2), and different enzymes (100 mU/mL ALP, 10 U/mL AChE, 10 U/mL esterase, 10 U/mL lipase, 10 U/mL lysozyme, and 10 U/mL trypsin, respectively) were incubated at 37 °C for 60 min. Ten microliters of the PEI-capped copper nanoclusters was added. The samples were mixed and the fluorescence signals were collected.

Alkaline phosphatase activity assay in biological fluid

A total volume of 390 μL of the sample mixtures containing 5% human serum, MnO_2 nanosheets (55 μg/mL), AAP (0.8 mM), phosphate buffer (5 mM, pH 8.2), and ALP at various concentrations was incubated at 37 °C for 60 min. Ten microliters of the PEI-capped copper nanoclusters was added. The samples were mixed and the fluorescence signals were collected.

Results and discussion

Synthesis and characterization of the PEI-capped CuNCs

PEI comprises many amino functional groups and has good affinity for metal ions. It provides and acts as a template and a protecting agent for the formation of nanomaterials, such as Au nanoparticles [43], Cu nanoclusters [44], and Ag nanoclusters [45]. We selected PEI (Mw = 10,000) as the capping ligand in the present study to synthesize the PEI-capped CuNCs. The as-prepared CuNCs exhibit good solubility in an aqueous solution. As shown in Fig. 1a, the NCs are mostly spherical in shape and display an average diameter of 1.8 nm. UV–Vis absorption spectrum illustrates that there is no characteristic surface plasmon band around 560–600 nm [29]. The results suggest that there are no large copper nanoparticles formed. As shown in Fig. 1b, the fluorescence

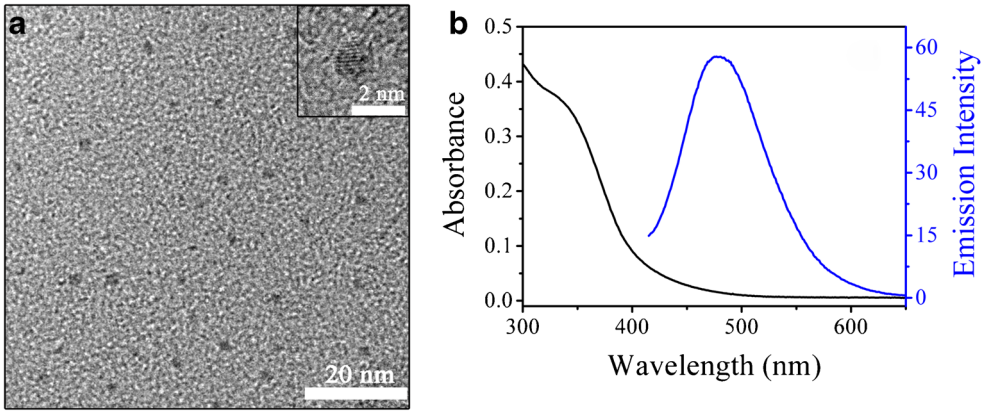

Fig. 1 (**a**) TEM images of the PEI-capped CuNCs. *Inset*: HRTEM image of the PEI-capped CuNCs. (**b**) UV–Vis absorption (*black*) and emission spectra (*blue*) of the CuNCs

emission spectrum of the CuNCs shows a peak centered at 475 nm upon excitation at 360 nm. Moreover, the emission intensity of the CuNCs was enhanced after the addition of a small amount of $NaBH_4$ (Electronic Supplementary Material (ESM), Fig. S1). The stability of the CuNCs was studied. As shown in Fig. S2 (see ESM), the emission intensity at 475 nm remained unchanged at different NaCl concentrations, and it showed minor decline at increasing assay solution pH values. After several temperature cycles, the fluorescence intensity did not vary, which demonstrates that the CuNCs are quite thermally stable.

Synthesis and characterization of the MnO_2 nanosheets

A facile procedure was adapted to prepare the MnO_2 nanosheets [34]. TEM and AFM results indicate that the newly prepared MnO_2 nanosheets exhibit typical 2D sheet-like morphology (Fig. 2a), with a thickness of about 0.8 nm (see ESM Fig. S3). UV–Vis absorption spectrum shows that the MnO_2 nanosheets have a wide absorption spectrum from 200 to 600 nm, with a characteristic peak at 360 nm (see ESM Fig. S4) [34]. A negative zeta potential value of −38.8 mV was obtained for the nanosheets as shown in Fig. S5 (see ESM), indicating negatively charged MnO_2 nanosheet surface.

Fluorescence quenching of the PEI-capped CuNCs by the MnO_2 nanosheets

PEI-capped CuNCs were selected as the fluorescence probe to detect ALP. They exhibit high cationic charge intensity due to the large number of amino groups on PEI, which can facilitate the electrostatic attractive interactions with the negatively charged MnO_2 nanosheets. Upon incubation of the CuNCs with the nanosheets, the NCs were easily adsorbed onto the surface of the nanosheets. Zeta potential measurement was used to monitor the surface charge of the MnO_2 nanosheets. As shown in Fig. S5 (see ESM), the addition of the CuNCs caused a significant change in surface potential from −38.8 to 8.34 mV, indicating the adsorption of the positively charged CuNCs. It was observed that the absorption spectrum of the MnO_2 nanosheets overlapped well with the fluorescence emission of the CuNCs (see ESM Fig. S4). Such a spectral overlap clearly demonstrates that the fluorescence emission of the CuNCs was quenched as a result of the resonance energy transfer from the NCs to the nanosheets. As shown in Fig. 3a, the emission of the CuNCs was efficiently quenched when mixed with the MnO_2 nanosheets. A decreased fluorescence intensity of the NCs at 475 nm was observed upon increasing the amount of the nanosheets. These findings clearly suggest that the fluorescence quenching efficiency is reliant on the

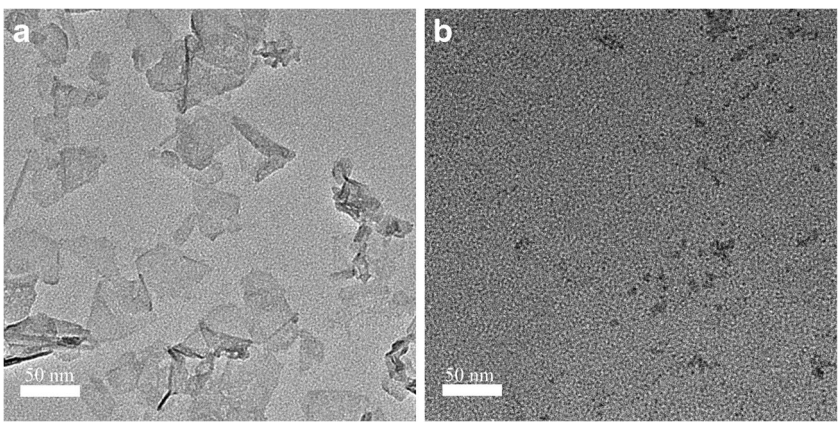

Fig. 2 TEM images of the MnO_2 nanosheets (**a**) and the nanosheets after the ALP enzymatic reaction (**b**)

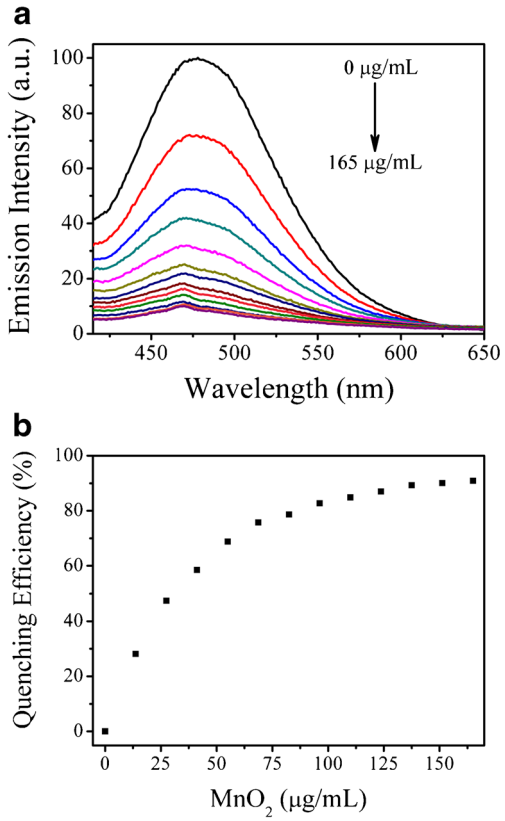

Fig. 3 (**a**) Emission spectral changes of the PEI-capped CuNCs as a function of the MnO_2 nanosheets concentration. (**b**) Fluorescence quenching efficiency at 475 nm versus MnO_2 nanosheets concentration

concentration of the MnO_2 nanosheet, and over 90% quenching efficiency was obtained when mixed with 165 μg/mL of the MnO_2 nanosheets (Fig. 3b).

ALP activity assay

The MnO_2 nanosheets can be reduced to Mn^{2+} in the presence of a proper reductant. The quenched fluorescence of the PEI-capped CuNCs increased gradually when mixed with increasing concentrations of AA (see ESM Fig. S6). The results demonstrate that AA could trigger the reduction of the MnO_2 nanosheets to Mn^{2+}. CuNCs were released, and recovery of the fluorescence of the CuNCs was observed.

AAP was hydrolyzed to AA via the catalysis of ALP. As shown in Fig. 2b, TEM image shows that no MnO_2 nanosheets were observed after the ALP enzymatic reaction. The characteristic UV–Vis absorption band of the MnO_2 nanosheets at 380 nm also disappeared completely (see ESM Fig. S7). The results directly corroborate that the MnO_2 nanosheets decomposed which was originated from the ALP catalyzed substrate hydrolysis.

The substrate concentration was optimized as shown in Fig. S8 (see ESM). When 0.8 mM 2-phospho-L-ascorbic acid was used, the fluorescence intensity changes (ΔF) reached maximum. As a result, 0.8 mM AAP was chosen for the subsequent experiments. The reaction time was examined as shown in Fig. S9 (see ESM). The emission intensity of the CuNCs increased gradually with gradually prolonged reaction time and reached its maximum at 60 min. Further increase in reaction time led to little changes in emission intensity of the CuNCs. Therefore, 60 min was selected as the optimal reaction time.

ALP activity was studied under the optimum conditions. The emission intensity of the CuNCs increased with increasing ALP concentration (0.5–200 mU/mL) (Fig. 4). The fluorescence emission intensity changes were proportional to the ALP concentration from 1 to 50 mU/mL. The linear regression equation is $IF = 43.16 + 0.91C$ ($R^2 = 0.99$), where "IF" represents the emission intensity of the CuNCs at 475 nm and C is the ALP concentration in milliunit per milliliter. The limit of detection (LOD) is estimated to be 0.27 mU/mL [13, 46–48].

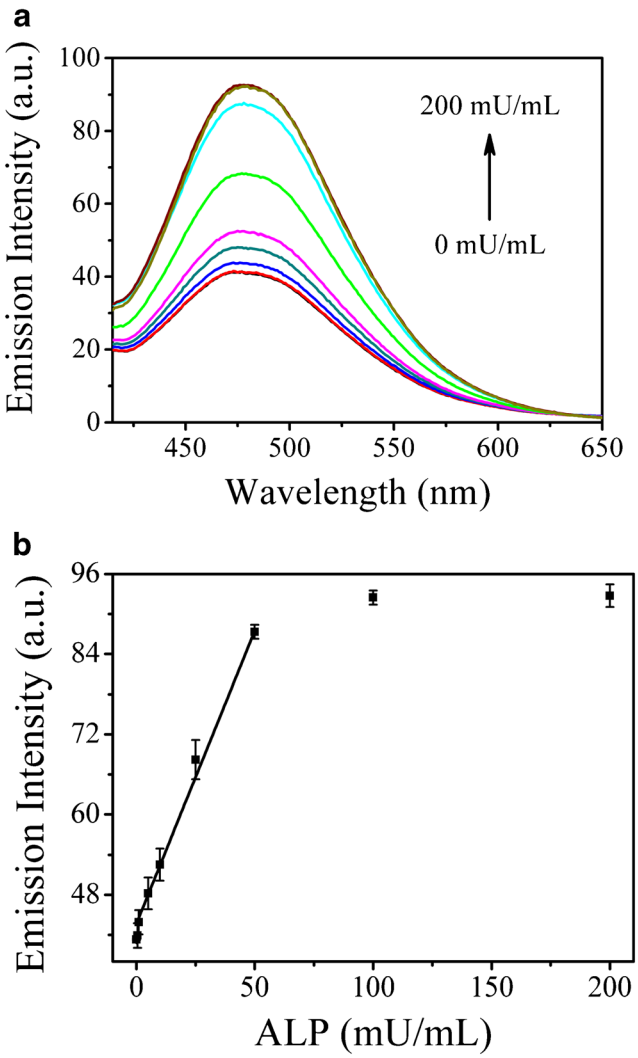

Fig. 4 (**a**) Changes in emission spectrum of the CuNCs upon the addition of ALP of different concentrations (0, 0.5, 1, 5, 10, 25, 50, 100, and 200 mU/mL). (**b**) CuNC emission intensity changes at 475 nm versus ALP concentration

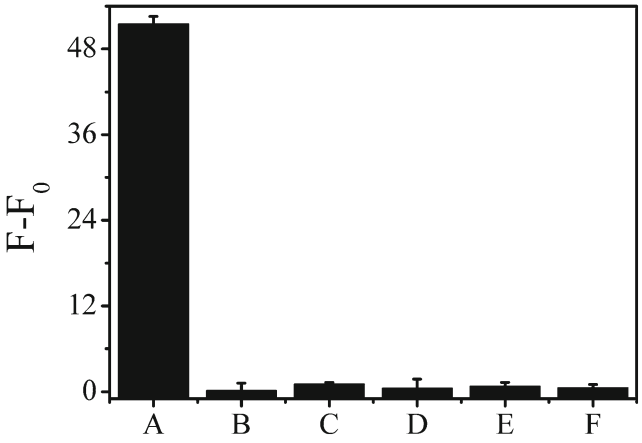

Fig. 5 Selectivity study. *Columns A–F*: ALP, AChE, esterase, lipase, lysozyme, and trypsin, respectively. ALP, 100 mU/mL; the other enzymes, 10 U/mL each. The emission intensity of the CuNCs at 475 nm was recorded, and background emission was subtracted for clarity

It should be noted that during the manuscript preparation process, a paper using a similar assay strategy for the detection of ALP was published [49]. The assay utilized carbon dots-MnO_2 nanocomposite as the probe is simple, economical, and green but requires high-temperature treatment (100 °C). Our assay contains a more detailed study on the electrostatic interactions of the PEI-Cu nanoclusters and the MnO_2 nanosheets (Fig. S5). In addition, more microscopic characterizations are included (Figs. 3 and S3). The results clearly show that the fluorescence of the CuNCs was quenched by the MnO_2 nanosheets, and the in situ generation of ascorbic acid caused decomposition of the nanosheets and turn-on fluorescence of the NCs.

Selectivity study

To further assess the specificity of our assay towards ALP, the selectivity experiments were carried out to test various possible interfering enzymes, including acetylcholinesterase (AChE), esterase, lipase, lysozyme, and trypsin. As shown in Fig. 5, a notable increase in emission intensity of the CuNCs was found in the presence of ALP. On the contrary, the other enzymes led to negligible optical responses even at a very high concentration (10 U/mL). The results reveal that these enzymes have no obvious interference and our sensing method is highly selective towards ALP.

ALP activity assay in biological fluid

To evaluate the effectiveness and suitability of the method for complex sample system, we applied it to a sample mixture containing dilute human serum (5%). As shown in Fig. S10 (see ESM), under the same experimental conditions, the emission recovery of the CuNCs was enhanced upon the addition of increasing concentrations of ALP. These findings strongly demonstrate that our method could be employed in biological fluids.

Conclusions

In summary, we have developed a novel method for fluorescence "turn-on" detection of ALP. In the sensing system, the PEI-capped CuNCs were employed as the fluorescence unit and the MnO_2 nanosheets were used as fluorescence quencher. In an aqueous solution, the MnO_2 nanosheets could adsorb the oppositely charged CuNCs. The fluorescence of the CuNCs was quenched efficiently as a result of energy transfer from the NCs to the nanosheets. In addition, ALP catalyzed the hydrolysis of AAP to produce AA, which could reduce MnO_2 to Mn^{2+}, and triggered the decomposition of the MnO_2 nanosheets. As a consequence, the CuNCs were released, a turn-on fluorescence signal was observed, and a simple, sensitive, and efficient sensing strategy for ALP detection was established. Our assay possesses several impressive features. The MnO_2 nanosheets and the CuNCs could be easily fabricated. More importantly, the use of simple and inexpensive materials makes the assay cost-effective. The sensor is simple in design and preparation and can also be used in complex sample system. Due to the better biocompatibility, the assay could be easily extended to ALP activity-related biological and biomedical applications.

Acknowledgments This work was supported by the National Natural Science Foundation of China (21561162004, 21550110196, 21374077, and 51573131), the Natural Science Foundation of Jilin Province (20150101183JC), the Hong Kong Research Grants Council and the National Natural Science Foundation of China (N_CityU113/15), and the Science and Technology Development Project of Jilin Province (International Collaboration Program, 20160414040GH).

Compliance with ethical standards

Conflict of interest The authors declare that they have no conflict of interest.

Human and animal rights and informed consent No violation of human and animal rights occurred during this investigation.

References

1. Coleman JE. Structure and mechanism of alkaline-phosphatase. Annu Rev Bioph Biom Struct. 1992;21:441–83.
2. Lalles JP. Intestinal alkaline phosphatase: novel functions and protective effects. Nutr Rev. 2014;72(2):82–94.
3. Goldberg DM, Martin JV, Knight AH. Elevation of serum alkaline-phosphatase activity and related enzymes in diabetes-mellitus. Clin Biochem. 1977;10(1):8–11.

4. Sardiwal S, Magnusson P, Goldsmith DJ, Lamb EJ. Bone alkaline phosphatase in CKD-mineral bone disorder. Am J Kidney Dis. 2013;62(4):810–22.
5. Lorente JA, Valenzuela H, Morote J, Gelabert A. Serum bone alkaline phosphatase levels enhance the clinical utility of prostate specific antigen in the staging of newly diagnosed prostate cancer patients. Eur J Nucl Med. 1999;26(6):625–32.
6. Colombatto P, Randone A, Civitico G, Gorin JM, Dolci L, Medaina N, et al. Hepatitis G virus RNA in the serum of patients with elevated gamma glutamyl transpeptidase and alkaline phosphatase: a specific liver disease. J Viral Hepatitis. 1996;3(6):301–6.
7. Jiao H, Chen J, Li W, Wang F, Zhou H, Li Y, et al. Nucleic acid-regulated perylene probe-induced gold nanoparticle aggregation: a new strategy for colorimetric sensing of alkaline phosphatase activity and inhibitor screening. ACS Appl Mater Interfaces. 2014;6(3):1979–85.
8. Yu L, Shi Z, Fang C, Zhang Y, Liu Y, Li C. Disposable lateral flow-through strip for smartphone-camera to quantitatively detect alkaline phosphatase activity in milk. Biosens Bioelectron. 2015;69:307–15.
9. Goggins S, Naz C, Marsh BJ, Frost CG. Ratiometric electrochemical detection of alkaline phosphatase. Chem Commun. 2015;51(3):561–4.
10. Zhang N, Ma ZY, Ruan YF, Zhao WW, Xu JJ, Chen HY. Simultaneous photoelectrochemical immunoassay of dual cardiac markers using specific enzyme tags: a proof of principle for multiplexed bioanalysis. Anal Chem. 2016;88(4):1990–4.
11. Wang W, Ouyang H, Yang S, Wang L, Fu Z. Multiplexed detection of two proteins by a reaction kinetics-resolved chemiluminescence immunoassay strategy. Analyst. 2015;140(4):1215–20.
12. Ruan CM, Wang W, Gu BH. Detection of alkaline phosphatase using surface-enhanced Raman spectroscopy. Anal Chem. 2006;78(10):3379–84.
13. Deng J, Yu P, Wang Y, Mao L. Real-time ratiometric fluorescent assay for alkaline phosphatase activity with stimulus responsive infinite coordination polymer nanoparticles. Anal Chem. 2015;87(5):3080–6.
14. Li Y, Zhou H, Chen J, Shahzad SA, Yu C. Controlled self-assembly of small molecule probes and the related applications in bioanalysis. Biosens Bioelectron. 2016;76:38–53.
15. Chen J, Jiao H, Li W, Liao D, Zhou H, Yu C. Real-time fluorescence turn-on detection of alkaline phosphatase activity with a novel perylene probe. Chem Asian J. 2013;8(1):276–81.
16. Wu N, Lan J, Yan L, You J. A sensitive colorimetric and fluorescent sensor based on imidazolium-functionalized squaraines for the detection of GTP and alkaline phosphatase in aqueous solution. Chem Commun. 2014;50(34):4438–41.
17. Zhu Y, Wang G, Jiang H, Chen L, Zhang X. One-step ultrasonic synthesis of graphene quantum dots with high quantum yield and their application in sensing alkaline phosphatase. Chem Commun. 2015;51(5):948–51.
18. Barroso J, Saa L, Grinyte R, Pavlov V. Photoelectrochemical detection of enzymatically generated CdS nanoparticles: application to development of immunoassay. Biosens Bioelectron. 2016;77:323–9.
19. Si Y, Sun Z, Zhang N, Qi W, Li S, Chen L, et al. Ultrasensitive electroanalysis of low-level free microRNAs in blood by maximum signal amplification of catalytic silver deposition using alkaline phosphatase-incorporated gold nanoclusters. Anal Chem. 2014;86(20):10406–14.
20. Li J, Zhu J-J, Xu K. Fluorescent metal nanoclusters: from synthesis to applications. Trends Anal Chem. 2014;58:90–8.
21. Zhang L, Wang E. Metal nanoclusters: new fluorescent probes for sensors and bioimaging. Nano Today. 2014;9(1):132–57.
22. Tao Y, Li M, Ren J, Qu X. Metal nanoclusters: novel probes for diagnostic and therapeutic applications. Chem Soc Rev. 2015;44(23):8636–63.
23. Jia XF, Li J, Han L, Ren JT, Yang X, Wang EK. DNA-hosted copper nanoclusters for fluorescent identification of single nucleotide polymorphisms. ACS Nano. 2012;6(4):3311–7.
24. Gao X, Lu Y, Liu M, He S, Chen W. Sub-nanometer sized $Cu_6(GSH)_3$clusters: one-step synthesis and electrochemical detection of glucose. J Mater Chem C. 2015;3(16):4050–6.
25. Liu X, Wang F, Aizen R, Yehezkeli O, Willner I. Graphene oxide/nucleic-acid-stabilized silver nanoclusters: functional hybrid materials for optical aptamer sensing and multiplexed analysis of pathogenic DNAs. J Am Chem Soc. 2013;135(32):11832–9.
26. Chen Y, Li W, Wang Y, Yang X, Chen J, Jiang Y, et al. Cysteine-directed fluorescent gold nanoclusters for the sensing of pyrophosphate and alkaline phosphatase. J Mater Chem C. 2014;2(20):4080–5.
27. Yuan Z, Cai N, Du Y, He Y, Yeung ES. Sensitive and selective detection of copper ions with highly stable polyethyleneimine-protected silver nanoclusters. Anal Chem. 2014;86(1):419–26.
28. Wu Z, Liu J, Gao Y, Liu H, Li T, Zou H, et al. Assembly-induced enhancement of Cu nanoclusters luminescence with mechanochromic property. J Am Chem Soc. 2015;137(40):12906–13.
29. Wei W, Lu Y, Chen W, Chen S. One-pot synthesis, photoluminescence, and electrocatalytic properties of subnanometer-sized copper clusters. J Am Chem Soc. 2011;133(7):2060–3.
30. Hu X, Liu T, Zhuang Y, Wang W, Li Y, Fan W, et al. Recent advances in the analytical applications of copper nanoclusters. Trends Anal Chem. 2016;77:66–75.
31. Jin L, Zhang Z, Tang A, Li C, Shen Y. Synthesis of yeast extract-stabilized Cu nanoclusters for sensitive fluorescent detection of sulfide ions in water. Biosens Bioelectron. 2016;79:108–13.
32. Zheng X-J, Liang R-P, Li Z-J, Zhang L, Qiu J-D. One-step, stabilizer-free and green synthesis of Cu nanoclusters as fluorescent probes for sensitive and selective detection of nitrite ions. Sens. Actuators. B. 2016;230:314–9.
33. Fan H, Yan G, Zhao Z, Hu X, Zhang W, Liu H, et al. A smart photosensitizer-manganese dioxide nanosystem for enhanced photodynamic therapy by reducing glutathione levels in cancer cells. Angew Chem Int Ed. 2016;55(18):5477–82.
34. Zhao Z, Fan H, Zhou G, Bai H, Liang H, Wang R, et al. Activatable fluorescence/MRI bimodal platform for tumor cell imaging via MnO_2 nanosheet-aptamer nanoprobe. J Am Chem Soc. 2014;136(32):11220–3.
35. Lu M, Qu J, Yao Q, Xu C, Zhan Y, Xie J, et al. Exploring metal nanoclusters for lithium-oxygen batteries. ACS Appl Mater Interfaces. 2015;7(9):5488–96.
36. Pan L, Wang K-X, Zhu X-D, Xie X-M, Liu Y-T. Hierarchical assembly of SnO_2 nanowires on MnO_2 nanosheets: a novel 1/2D hybrid architecture for high-capacity, reversible lithium storage. J Mater Chem A. 2015;3(12):6477–83.
37. Kai K, Yoshida Y, Kageyama H, Saito G, Ishigaki T, Furukawa Y, et al. Room-temperature synthesis of manganese oxide monosheets. J Am Chem Soc. 2008;130(47):15938–43.
38. Chen Y, Ye D, Wu M, Chen H, Zhang L, Shi J, et al. Break-up of two-dimensional MnO_2 nanosheets promotes ultrasensitive pH-triggered theranostics of cancer. Adv Mater. 2014;26(41):7019–26.
39. Deng R, Xie X, Vendrell M, Chang YT, Liu X. Intracellular glutathione detection using MnO_2-nanosheet-modified upconversion nanoparticles. J Am Chem Soc. 2011;133(50):20168–71.
40. He D, He X, Wang K, Yang X, Yang X, Li X, et al. Nanometer-sized manganese oxide-quenched fluorescent oligonucleotides: an effective sensing platform for probing biomolecular interactions. Chem Commun. 2014;50(75):11049–52.

41. Zhang XL, Zheng C, Guo SS, Li J, Yang HH, Chen G. Turn-on fluorescence sensor for intracellular imaging of glutathione using g-C_3N_4 nanosheet-MnO_2 sandwich nanocomposite. Anal Chem. 2014;86(7):3426–34.
42. Yuan Y, Wu S, Shu F, Liu Z. An MnO_2 nanosheet as a label-free nanoplatform for homogeneous biosensing. Chem Commun. 2014;50(9):1095–7.
43. Wen S, Zheng F, Shen M, Shi X. Synthesis of polyethyleneimine-stabilized gold nanoparticles for colorimetric sensing of heparin. Colloids Surf A Physicochem Eng Asp. 2013;419:80–6.
44. Ling Y, Wu JJ, Gao ZF, Li NB, Luo HQ. Enhanced emission of polyethyleneimine-coated copper nanoclusters and their solvent effect. J Phys Chem C. 2015;119(48):27173–7.
45. Qu F, Li NB, Luo HQ. Highly sensitive fluorescent and colorimetric pH sensor based on polyethylenimine-capped silver nanoclusters. Langmuir. 2013;29(4):1199–205.
46. Li G, Fu H, Chen X, Gong P, Chen G, Xia L, et al. Facile and sensitive fluorescence sensing of alkaline phosphatase activity with photoluminescent carbon dots based on inner filter effect. Anal Chem. 2016;88(5):2720–6.
47. Dong L, Miao Q, Hai Z, Yuan Y, Liang G. Enzymatic hydrogelation-induced fluorescence turn-off for sensing alkaline phosphatase in vitro and in living cells. Anal Chem. 2015;87(13):6475–8.
48. Lin JH, Yang YC, Shih YC, Hung SY, Lu CY, Tseng WL. Photoinduced electron transfer between Fe(III) and adenosine triphosphate-BODIPY conjugates: application to alkaline-phosphatase-linked immunoassay. Biosens Bioelectron. 2016;77:242–8.
49. Qu F, Pei H, Kong R, Zhu S, Xia L. Novel turn-on fluorescent detection of alkaline phosphatase based on green synthesized carbon dots and MnO_2 nanosheets. Talanta. 2017;165:136–42.